Accepted Manuscript

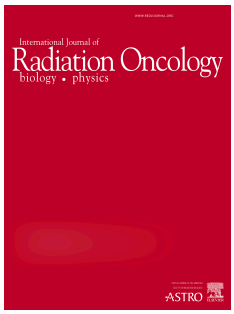

Spatial comparison of CT-based surrogates of lung ventilation with hyperpolarized Helium-3 and Xenon-129 gas MRI in patients undergoing radiation therapy

B.A. Tahir, PhD, P.J.C. Hughes, MEng, S.D. Robinson, MD, H. Marshall, PhD, N.J. Stewart, PhD, G. Norquay, PhD, A. Biancardi, PhD, H.-F. Chan, MEng, G.J. Collier, PhD, K.A. Hart, MSc, J.A. Swinscoe, PhD, M.Q. Hatton, MD, J.M. Wild, PhD, R.H. Ireland, PhD

PII: S0360-3016(18)30755-7

DOI: 10.1016/j.ijrobp.2018.04.077

Reference: ROB 24986

To appear in: *International Journal of Radiation Oncology • Biology • Physics*

Received Date: 28 December 2017

Revised Date: 21 March 2018

Accepted Date: 26 April 2018

Please cite this article as: Tahir B, Hughes P, Robinson S, Marshall H, Stewart N, Norquay G, Biancardi A, Chan H-F, Collier G, Hart K, Swinscoe J, Hatton M, Wild J, Ireland R, Spatial comparison of CT-based surrogates of lung ventilation with hyperpolarized Helium-3 and Xenon-129 gas MRI in patients undergoing radiation therapy, *International Journal of Radiation Oncology • Biology • Physics* (2018), doi: 10.1016/j.ijrobp.2018.04.077.

This is a PDF file of an unedited manuscript that has been accepted for publication. As a service to our customers we are providing this early version of the manuscript. The manuscript will undergo copyediting, typesetting, and review of the resulting proof before it is published in its final form. Please note that during the production process errors may be discovered which could affect the content, and all legal disclaimers that apply to the journal pertain.

ACCEPTED MANUSCRIPT

Title Page

Spatial comparison of CT-based surrogates of lung ventilation with hyperpolarized Helium-3 and Xenon-129 gas MRI in patients undergoing radiation therapy

Short Title

Spatial comparison of CT- and gas MR-ventilation

Authors and Affiliations

Tahir BA[1,2], PhD, Hughes PJC[2], MEng, Robinson SD[1,2], MD, Marshall H[2], PhD, Stewart NJ[2], PhD, Norquay G[2], PhD, Biancardi A[2], PhD, Chan H-F[2], MEng, Collier GJ[2], PhD, Hart KA[1], MSc, Swinscoe JA[1], PhD, Hatton MQ[1], MD, Wild JM[2], PhD, and Ireland RH[1,2], PhD
[1]Academic Unit of Clinical Oncology and [2]POLARIS, Academic Radiology, University of Sheffield, UK

Corresponding Author/Author responsible for statistical analysis

Bilal A. Tahir, PhD,

Academic Unit of Clinical Oncology,

Weston Park Hospital,

University of Sheffield,

Sheffield S10 2JF,

United Kingdom

b.tahir@sheffield.ac.uk

Acknowledgements

This work was supported by the University of Sheffield James Morrison Fund, Sheffield Hospitals Charity, Weston Park Hospital Cancer Charity and National Institute of Health Research.

Disclosure

No conflict of interest

ACCEPTED MANUSCRIPT

Spatial comparison of CT-based surrogates of lung ventilation with hyperpolarized Helium-3 and Xenon-129 gas MRI in patients undergoing radiation therapy

Purpose: To develop and apply an image acquisition and analysis strategy for spatial comparison of CT-ventilation images with hyperpolarized gas MRI.

Methods: 11 lung cancer patients underwent ^{129}Xe and ^{3}He ventilation MRI and co-registered ^{1}H anatomical MRI. Expiratory and inspiratory breath-hold CTs were used for deformable image registration and calculation of three CT-ventilation metrics: Hounsfield unit (CT^{HU}), Jacobian (CT^{Jac}) and specific gas volume change (CT^{SGV}). Inspiration CT and hyperpolarized gas ventilation MRI were registered via same-breath anatomical ^{1}H-MRI. Voxel-wise Spearman correlation coefficients were calculated between each CT-ventilation image and its corresponding ^{3}He/^{129}Xe-MRI, and for the mean values in regions of interest (ROIs) ranging from fine to coarse in-plane dimensions of 5x5, 10x10, 15x15 and 20x20, located within the lungs as defined by the same-breath ^{1}H-MRI lung mask. Correlation of ^{3}He and ^{129}Xe-MRI was also assessed.

Results: Spatial correlation of CT-ventilation against ^{3}He/^{129}Xe-MRI increased with ROI size. For example, for CT^{HU}, mean±SD Spearman coefficients were 0.37±0.19/0.33±0.17 at the voxel-level and 0.52±0.20/0.51±0.18 for 20x20 ROIs, respectively. Correlations were stronger for CT^{HU} than for CT^{Jac} or CT^{SGV}. Correlation of ^{3}He with ^{129}Xe-MRI was consistently higher than either gas against CT-ventilation maps over all ROIs ($p<0.05$). No significant differences were observed between CT-ventilation vs ^{3}He-MRI and CT-ventilation vs ^{129}Xe-MRI.

Conclusion: Comparison of ventilation-related measures from CT and registered hyperpolarized gas MRI is feasible at a voxel level using a dedicated acquisition and analysis protocol. Moderate correlation between CT-ventilation and MRI exists at a regional level. Correlation between MRI and CT is significantly less than between ^{3}He and ^{129}Xe-MRI, suggesting that CT-ventilation surrogate measures may not be measuring lung ventilation alone.

1. Introduction

When planning lung cancer radiation therapy, knowledge of pulmonary ventilation and perfusion can help spare functional lung tissue and reduce the impact of the dose limiting toxicities of pneumonitis and pulmonary fibrosis [25]. Such functional lung avoidance treatment planning has been most frequently investigated using single photon emission computed tomography

(SPECT) [11,40], although studies using helium-3 magnetic resonance imaging (^{3}He-MRI) [24,45] and positron emission tomography (PET) [41,42] have also been reported.

As computed tomography (CT), and increasingly 4D-CT, is the default modality for treatment planning, recent efforts have focused on developing an alternative modality for functional lung avoidance planning. CT-based surrogates of regional ventilation, often referred to as 'CT-ventilation maps', are derived from pulmonary CT images acquired at different inflation levels, without the use of exogenous contrast, by assuming that regional changes in lung volume relate to regional ventilation. Several methodologies exist to compute these surrogates, including use of the determinant of the Jacobian [39], a direct geometrical calculation [55,56], and lung density changes computed directly from CT intensity [18]. Currently, CT-ventilation is the subject of three functional lung avoidance radiotherapy trials (NCT02528942, NCT02308709, NCT02843568).

A central focus of enquiry in the field of CT-based ventilation investigations has been the validation of the modality against more established measures of pulmonary function. Comparing CT ventilation-derived metrics such as defective lung volumes and coefficients of variation with global measurements of spirometry, moderate correlations between FEV_1 and FEV/FVC, ranging from 0.43 to 0.73 and 0.38 to 0.73 for the intensity and Jacobian metrics have been reported, respectively [6,54]. In animal experiments, CT-based ventilatory surrogates have demonstrated both a reasonably high level (Jacobian metric, linear regression = 0.73 [39]; intensity metric, correlation coefficient = 0.66 [15]; hybrid metric, correlation coefficient = 0.82, [13]) and relatively low level (geometric metric, Spearman coefficient = 0.44 [57]) of correlation with contrast enhanced Xenon-CT. However, the subjects were mechanically ventilated and the Xenon-CT used had limited axial coverage thus limiting its ability to provide a validation over the full lung volume. Recently, a high correlation of 0.89 ($p<0.0001$) has been observed in rats against Cryomicrotome imaging after exposure to aerosols of 1μm fluorescent

microspheres (FMS) [27]. However, the ground truth image requires ex-vivo dissection of the lung, prohibiting its use in human subjects.

In light of these difficulties, the vast majority of validation studies in humans have compared the technique against nuclear medicine-based imaging using both planar and tomographic configurations, with conflicting results reported in the literature (dice coefficient = 0.35 [9]; dice coefficient = 0.39 [54]; correlation coefficient = 0.66 [49]). Although regional lung function has traditionally been assessed by nuclear imaging, it suffers from poor accuracy, spatial and temporal resolution and aerosol depositions in defect regions [38] and is thus not the optimal modality for a valid comparison.

The efficacy of ventilation-based nuclear imaging can be improved by positron emission tomography (PET) by inhalation of Gallium-68 carbon nanoparticles, commonly referred to as Galligas, and has shown moderate correlations with 4D-CT [28,29]. However, although the imaging data of these studies were acquired to enable improvements over 4D-CT ventilation vs SPECT studies with 4D-CT acquired at the same session and couch as PET, inherent discrepancies in image acquisition settings still remained. In general, the PET Galligas ventilation images in those studies were acquired over a minimum time scale of 10 minutes to ensure sufficient accumulation of the tracer, increasing for poor inhalations or low administered doses [7]. By contrast, 4D-CT is acquired over a single tidal breath. Such differences may reduce spatial correlations between the two modalities.

Hyperpolarized gas MR imaging is an alternative technique to nuclear imaging that can provide exquisite images of ventilation with superior spatial resolution, without the use of ionising radiation. Furthermore, it possesses improved temporal resolution to enable image acquisition in a single breath-hold. Gas MRI has been applied to the study of many respiratory diseases including lung cancer [24] and is a viable candidate as a reference modality.

Previously, Mathew et al. [34] evaluated the spatial correspondence of 4D-CT ventilation derived from the intensity based metric with ^{3}He MRI for eleven

lung cancer patients. However, this work had several methodological limitations. Firstly, the image acquisition protocol was not optimised to minimise potential discrepancies between the two modalities; the two different scans were acquired at a mean interval of 1.5 weeks for each patient and thus some of the regional ventilation differences in their study could be attributable to disease progression and time-related physiological differences. Furthermore, differences in patient positioning (treatment planning couch vs diagnostic MRI couch) and breathing maneuver (inspiratory breath-hold vs tidal breathing) were not explicitly accounted for, potentially leading to differences in the imaged physiologic states and registration errors. Ireland et al. [26] demonstrated significant improvements in rigid registration by reproducing the same breath-hold and body positions during image acquisition of CT and ^{3}He MRI. Secondly, only fiducial anatomical landmark affine registration was used to ensure the CT-ventilation and HP gas images were in the same spatial domain without accounting for deformable differences between the two images, owing to postural differences. Thirdly, only ventilation derived from an intensity metric was evaluated in this study with no reference to other prominent metrics such as the Jacobian metric. Fourthly, the assessment of spatial correlation was limited to spatial overlap analysis of binary thresholded images. Such overlap measures provide a more global comparison and thus voxel-wise and region of interest (ROI) analysis may improve the comparison by assessing the correlation of the intensity distribution of corresponding regions within the binary segmentations.

Although hyperpolarized gas imaging with ^{3}He has demonstrated superb visualisation of pulmonary airspaces, due to the limited and unpredictable global supplies of ^{3}He, ^{129}Xe has begun to play a more important role in recent years [36]. To date, no published study has investigated the spatial correlation of the CT-based ventilation techniques against ^{129}Xe MRI. Similarly, although a number of studies have emerged in the past few years comparing ^{3}He and ^{129}Xe MR techniques for imaging ventilation [44] and microstructure [30], only global means of comparison such as the percent

ACCEPTED MANUSCRIPT

ventilated volume have been used and voxel-wise and more regional forms of analysis are yet to be performed.

Appendix A summarises previous studies comparing CT-ventilation against other pulmonary functional imaging modalities.

The primary objective of this study, therefore, was to develop an image acquisition and analysis strategy to minimize differences between functional imaging modalities and hence optimize the accuracy of regional correlation analysis. The strategy was tested with two types of hyperpolarized gas MRI, ^{3}He and ^{129}Xe, a rapidly emerging technology that provides detailed and direct maps of lung ventilation.

2. Methods and Materials

2.1 Patients

Thirteen patients with non-small cell lung cancer provided written informed consent for an institutional review board-approved, single-institution, prospective, single-arm clinical study (ClinicalTrials.gov: **Anonymized**). The inclusion criteria were greater than 18 years of age, a multidisciplinary team diagnosis of NSCLC based on findings of positive histology, positive PET scan or growth on serial CT scans and ability to tolerate MRI scanning. The exclusion criteria included co-morbid conditions that exclude radiotherapy treatment, inability to give informed consent and women who are pregnant or of child-bearing potential.

2.2 CT

Patients underwent expiration and inspiration breath-hold CT at functional residual capacity (FRC) and FRC+1L, respectively, on a 16-slice Lightspeed CT (GE Healthcare, Princeton, NJ). Each acquisition was acquired within 15 to 20 seconds. The inspiratory breath-hold was performed with a 1L Tedlar

bag filled with room air that enabled simulation of the subsequent MRI breathing maneuver. Patients were coached on how to perform breathing maneuvers prior to imaging. Patients were immobilized on a radiotherapy wing board in conventional supine planning position with arms raised above the head. Inspiratory breath-hold was performed by inhaling 1L from a Tedlar bag filled with room air to mimic the equivalent hyperpolarized gas MR breath-hold. CT settings were: tube voltage=120kV, tube current=315mA, in-plane resolution 0.98×0.98mm, pixel matrix 512×512, slice thickness=2.5mm.

2.3 MRI

On the same day as CT, patients underwent MRI on a 1.5T scanner (GE HDx, GE Healthcare, Milwaukee, WI) in the treatment planning position using a custom-built radiotherapy wing board and flat-bed insert to mimic CT positioning. Separate flexible quadrature radiofrequency coils were employed for transmission and reception of MR signals at the respective Larmor frequencies of ^{3}He and ^{129}Xe (Clinical MR Solutions, Brook-field, WI). Hyperpolarized ^{3}He and ^{129}Xe gases were polarized to approximately 25% using a prototype commercial spin-exchange optical pumping polarizer (GE Healthcare, Amersham, UK), and a home-built system [35], respectively.

Firstly, ^{129}Xe (600mL of 129-enriched Xe gas and 400mL N_2) and matching anatomical ^{1}H-MRI were acquired in separate breath-holds at the same inflation state as inspiratory CT. During a changeover period of approximately 15 minutes to allow for ^{3}He radiofrequency coil setup, patients were moved off the couch. Subsequently, ^{3}He (200mL ^{3}He and 800mL N_2) and ^{1}H-MRI were acquired, also at the same inflation state as inspiratory CT but in a single breath-hold [22,50,51].

^{129}Xe ventilation MRI was acquired using a 3D steady-state free precession sequence, 4x4mm^2 in-plane resolution, 10mm slice thickness, 40cm field of view, 2.2ms echo time, 6.7ms repetition time, 10□ flip angle, ±8kHz bandwidth and whole-lung coverage (20 to 24 slices). ^{3}He ventilation MRI was also acquired with a 3D steady-state free precession sequence with

parameters as above except: 5mm slice thickness, 0.6ms echo time, 1.9ms repetition time, ±83.3kHz bandwidth and 40 to 48 slices. ^{129}Xe-MRI and ^{3}He-MRI were acquired within 15 and 7 seconds, respectively. The reproducibility of the ^{3}He and ^{129}Xe-MRI sequences used in this study has previously been observed to be on the same order of magnitude as spirometry [43]**.**

Corresponding separate and same-breath anatomical ^{1}H images [50] were acquired with equivalent spatial resolution as ^{129}Xe and ^{3}He images using the ^{1}H transmit-receive body coil of the scanner with the following settings: 3D spoiled gradient echo, 0.6ms echo time, 1.9ms repetition time, 5□ flip angle, and ±83kHz bandwidth.

2.4 Image segmentation

For subsequent processing steps including image registration, CT lung parenchyma was segmented using the Eclipse treatment planning system (Varian Medical Systems, Palo Alto, CA) and ^{1}H-MR lung parenchyma was segmented using Spatial Fuzzy C-means [23]. CT and MRI segmentations were manually edited where errors were present.

2.5 Image registration

Image registration was performed using the `antsRegistration` tool [3,4] and quantitatively evaluated using dice similarity coefficients (DSCs) between the registered expiratory to inspiratory CT and inspiratory CT to ^{1}H-MRI lung masks. **Appendix B** describes the parameters used.

For each patient, three image registrations were performed:

1) Expiratory CT to inspiratory CT
2) Inspiratory CT to ^{3}He-MRI's same breath ^{1}H-MRI
3) ^{129}Xe-MRI's separate breath ^{1}H-MRI to ^{3}He-MRI's same breath ^{1}H-MRI.

Each registration pipeline consisted of rigid, affine and diffeomorphic stages.

As the ^{129}Xe-MRI and its corresponding separate breath anatomical ^{1}H-MRI were acquired in the same inflation state (FRC+1L), they were assumed to be initially spatially co-registered. This was checked for each patient. Consequently, the same transform to map ^{129}Xe-MRI's separate breath ^{1}H-MRI to ^{3}He-MRI's same breath ^{1}H-MRI was applied to map ^{129}Xe-MRI to ^{1}H-MRI with linear interpolation.

2.6 CT-ventilation mapping computation

Three methods for generating voxel-wise CT surrogates of regional ventilation were investigated: Hounsfield unit (HU) change (CT^{HU}), specific gas volume change (CT^{SGV}), and Jacobian determinant of the deformation field (CT^{Jac}). To facilitate a direct spatial comparison of CT-ventilation and hyperpolarized gas MRI, all CT-ventilation images were generated at inhalation CT geometry as the latter was acquired at the same level of inflation as MRI (FRC+1L).

(i) CT^{HU} was computed from voxel-wise intensity differences in HU based on a modified version of the original formulation of Guerrero et al. [18] to account for the computation being performed in the inhalation CT spatial domain:

$$\frac{\Delta V}{V_{exp}} = 1000 \frac{HU_{ins} - \overline{HU}_{exp}}{\overline{HU}_{exp}(1000 + HU_{ins})}$$

where $\overline{HU}_{exp}$ is the average HU of the voxels in the moving deformed expiration image which spatially correspond to the voxels in the fixed inspiration image and HU_{insp} is the HU of the inspiratory voxel. CT^{HU} purports to be a measure of change in fractional content of air per voxel between respiratory phases. It is based on the assumption that uniform air distribution exists in a given parenchymal unit and that the change in volume between respiratory phases is attributable to changes in air volume only (i.e. tissue is incompressible and there is no change in the volume of tissue between inspiration and expiration)."

(ii) CT^{SGV} was computed from voxel-wise differences in specific gas volume (ΔSGV) between the warped expiration ($\overline{SGV_{exp}}$) and fixed inspiration image (SGV_{ins}) [2]:

$$\Delta SGV = SGV_{ins} - \overline{SVG}_{exp}$$

Specific gas volume was initially proposed by Coxson et al. [12] and is defined in units of millilitres of gas volume per gram of tissue (ml/g). For each inhalation level:

$$SGV = specific\ volume_{gas\&tissue} - specific\ volume_{tissue}$$

The specific volume of tissue is assumed to be constant, regardless of inflation level, and is equivalent to 0.94 ml/g [21]. The specific volume of gas and tissue is computed directly from thoracic CT images:

$$specific\ volume_{gas\&tissue} = \frac{1024}{HU+1024}$$

(iii) CT^{Jac} was calculated directly on the inversely consistent deformation field of expiratory CT to inspiratory CT by computing the Jacobian determinant (J) of the deformation field $h(x, y, z)$:

$$J\big(h(x,y,z)\big) = \begin{vmatrix} 1+\frac{\partial h_x(x,y,z)}{\partial x} & \frac{\partial h_x(x,y,z)}{\partial y} & \frac{\partial h_x(x,y,z)}{\partial z} \\ \frac{\partial h_y(x,y,z)}{\partial x} & 1+\frac{\partial h_y(x,y,z)}{\partial y} & \frac{\partial h_y(x,y,z)}{\partial z} \\ \frac{\partial h_z(x,y,z)}{\partial x} & \frac{\partial h_z(x,y,z)}{\partial y} & 1+\frac{\partial h_z(x,y,z)}{\partial z} \end{vmatrix}$$

The Jacobian determinant provides a measure of contraction and expansion such that a voxel value of one represents preservation of local volume, while values less than and greater than one correspond to contraction and expansion of local volume, respectively. To ensure that CT^{Jac} was spatially correlated to the other metrics, it was subsequently warped to the spatial

domain of inspiratory CT by applying the transform of expiratory CT to inspiratory CT with linear interpolation.

Further discussion on these techniques is provided in section 4.1.

2.7 Quantitative spatial comparison of CT-ventilation and hyperpolarized gas MRI

To ensure that the generated CT-ventilation images were in the same spatial domain as ^{3}He and the warped ^{129}Xe-MRI, the inspiratory CT to ^{1}H-MRI transform was applied to all CT-ventilation images [46]. This enabled a direct spatial comparison of CT-ventilation with both ^{3}He and ^{129}Xe-MRI (Figure 1). Spatial correlation was assessed by computing the voxel-wise Spearman correlation coefficients between each CT-ventilation image and its corresponding ^{3}He/^{129}Xe MR image, and for the mean values in regions of interest (ROIs), ranging from finer to coarser in-plane dimensions of 5x5, 10x10, 15x15 and 20x20, located within the lungs as defined by the same-breath ^{1}H-MRI lung mask.

To account for uncertainties in HU due to image noise and registration errors, previous studies have filtered the computed CT-ventilation images [9,10,18]. To investigate the effect of varying degrees of filtering on the spatial correlation of CT-ventilation and hyperpolarized gas MRI, the same analysis described above was performed with a median filter radius ranging from 1x1x1 to 7x7x7 voxels applied to the CT^{HU} image whereby the median filer was applied only to voxels within lung parenchyma as defined by the same-breath ^{1}H-MRI lung mask. To establish baseline Spearman correlation coefficient values when two similar ventilation imaging techniques are compared, Spearman coefficients were assessed between ^{3}He and ^{129}Xe-MRI at the voxel-level and for the same ROIs detailed above. Signal to noise ratios (SNRs) for images of both gases were also quantified.

2.8 Statistical analysis

Statistical analysis was performed using IBM SPSS software (version 20.0; Chicago, Il). A p-value<0.05 was considered statistically significant. Wilcoxon signed-rank test was used to assess the statistical significance of the differences between the Spearman correlation coefficients of the different CT-ventilation methods and hyperpolarized gas MRI for the voxel-wise and ROI analysis, the ^{3}He vs ^{129}Xe Spearman correlation coefficients compared to that of CT-ventilation vs ^{3}He and ^{129}Xe-MRI, and the difference between ^{3}He and ^{129}Xe-MRI SNR.

3. Results

3.1 Patients

From February 2015 to March 2017, thirteen patients were enrolled. One patient was unable to tolerate the MRI acquisition procedure and the data for another was excluded due to a truncated lung artefact whereby the entirety of the lungs was not captured in the inspiratory breath-hold image, leaving eleven patients (Table 1).

3.2 Image registration

Visual examination indicated accurate registration of the three registration pipelines in all cases. Quantitative overlap analysis demonstrated mean±SD DSCs for the expiratory to inspiratory CT and inspiratory CT to ^{1}H-MRI registrations of 0.99±0.00 and 0.98±0.00, respectively.

3.3 Spatial comparison of CT-ventilation and hyperpolarized gas MRI

Figure 2 shows corresponding coronal slices of the three CT-ventilation mapping methods tested here (CT^{HU}, CT^{SGV} and CT^{Jac}), where each is filtered with a median radius of 3x3x3 voxels, and ^{3}He and ^{129}Xe-MRI for three patient cases after image registration. These cases correspond to the best, intermediate and worst cases of correlation of CT-ventilation and

hyperpolarized gas MRI observed in this study. For the best case, a marked defect in the right lower lobe can be observed with all methods. Spatial correlation for all three CT-ventilation techniques with both ^{3}He (CT^{HU} = 0.8; CT^{SGV} = 0.7; CT^{Jac} = 0.7) and ^{129}Xe-MRI (CT^{HU} = 0.7; CT^{SGV} = 0.6; CT^{Jac} = 0.6) was strong and on the same order as the correlation of ^{3}He and ^{129}Xe-MRI (0.8). For the intermediate case, a similarly located ventilation defect can be observed in all images in the right upper lobe with varying degrees of spatial extent where hyperpolarized gas MRI exhibited a larger ventilation defect region than all CT-ventilation methods. Consequently, whereas the voxel-wise Spearman correlation coefficients of CT-ventilation against ^{3}He (CT^{HU} = 0.5; CT^{SGV} = 0.3; CT^{Jac} = 0.4) and ^{129}Xe-MRI (CT^{HU} = 0.5; CT^{SGV} = 0.3; CT^{Jac} = 0.4) were moderate for this patient, the coefficient between ^{3}He and ^{129}Xe was strong (0.7). For the worst case, CT-ventilation correlation was weak with both ^{3}He (CT^{HU} = 0.1; CT^{SGV} = 0.1; CT^{Jac} = 0.1) and ^{129}Xe-MRI (CT^{HU} = 0.1; CT^{SGV} = 0.2; CT^{Jac} = 0.1) whilst ^{3}He and ^{129}Xe-MRI also demonstrated strong correlation (0.8) with each other.

Figure 3 shows the Spearman correlation coefficients between CT^{HU} (median filter radius: 3x3x3 voxels) and ^{3}He and ^{129}Xe-MRI at the voxel level and for a range of corresponding ROIs of all patient data. For comparison, the results of the spatial comparison between ^{3}He and ^{129}Xe-MRI are also included. Spatial correlations between CT^{HU}, ^{3}He and ^{129}Xe increase with more coarsely defined ROIs and reach a plateau for an ROI of 15x15 voxels. Furthermore, Spearman correlation was stronger for ^{3}He vs ^{129}Xe-MRI compared with CT^{HU} vs either ^{3}He or ^{129}Xe-MRI. These observed differences were statistically significant over all ROIs ($p<0.05$) except between the 15x15 and 20x20 ROIs. No significant differences were observed between CT^{HU} vs ^{3}He-MRI and CT^{HU} vs ^{129}Xe-MRI. The mean±SD SNRs for ^{3}He and ^{129}Xe-MRI were 46.2±18.3 and 22.6±13.3, respectively; i.e. ^{3}He MRI consistently demonstrated higher SNR ($p<0.05$).

3.4 Effect of filtering

Figure 4 shows the effects of varying median filter sizes on the Spearman correlations of the CT^{HU} metric against both ^{3}He and ^{129}Xe-MRI. The application of filtering brings about a marked improvement in spatial correlation with hyperpolarized gas MRI compared with the unfiltered images. However, a plateau is reached at a median filter radius of 3x3x3 voxels whereby no significant increases in correlation coefficients ($p<0.05$) are observed thereafter. Performing the voxel-wise Spearman's analysis over increasing ROI sizes also results in increased correlation. A similar trend was observed as in Figure 3 where the increases are only marginal at larger ROI sizes of 15x15 and above.

Figure 5 summarises the effects of different CT-ventilation metrics and filtering settings on mean Spearman correlation coefficients of CT-ventilation against both ^{3}He and ^{129}Xe. A similar trend is observable as in Figure 4 where spatial correlation increases between images with increasing filter radiuses up to a median filter radius of 3x3x3 voxels for CT^{HU} with no significant differences observed thereafter ($p>0.05$). However, statistically significant differences were observed over all ROIs for CT^{SGV} and CT^{Jac} ($p<0.05$). The CT^{HU} metric performed significantly better than the other two metrics when filtering was applied. One exception should be noted; CT^{Jac} performed better than the other two metrics for the voxel-wise comparison when no filtering was applied.

4. Discussion

4.1 Correlation of CT-ventilation and hyperpolarized gas MRI

Moderately low correlations (r_s ~ 0.2-0.3) at the voxel-level were observed between CT-ventilation maps and both ^{3}He and ^{129}Xe-MRI, increasing to moderate (r_s ~ 0.3-0.5) correlation for coarser regions. This is consistent with a comparison of 4D-CT based ventilation with *ex vivo* Cryomicrotome imaging in rats [27], which showed improved correlations for larger ROIs. At the lobar

level, higher correlations have been demonstrated for ^{3}He-MRI [47] and PET Galligas ventilation scans [14]. Visual comparisons of CT-ventilation and MRI demonstrated similar ventilation defects but, in many cases, with varying extent. This may explain why CT-based surrogates of ventilation demonstrate increased correlation at coarser levels, as a larger ROI is influenced less by registration errors.

Similarly, increasing correlation at the voxel level was observed for increasing filter sizes, which is in line with previous studies comparing the effects of filtering on Spearman's correlation [28]. Correlation increased with increasing ROI size until a plateau was observed for filter sizes of 3x3x3 voxels and higher. This may be in part due to the fact that only the CT-ventilation images were filtered while the reference hyperpolarized gas MR images were not. However, ROI analysis was applied equally to all images.

This work highlights the importance of the minimum spatial resolution required for CT-ventilation. While it is often desirable to perform anatomic lung imaging at higher spatial resolutions, this is not necessarily the case for functional lung imaging. As noted by Levin et al. [32], functional lung images need only be acquired at the resolution of the smallest gas exchange unit, namely, the acinus (estimated to be on the order of 10x10x10mm^3), and that an even lower spatial resolution such as 20x20x20mm^3 is adequate for most applications due to functional defects demonstrating a tendency to be spatially clustered.

In agreement with previous studies [31,53], visual examination of ventilation images derived from the intensity (CT^{HU} and CT^{SGV}) and volume change (CT^{Jac}) based metrics indicated significant differences between the two methods that could be attributable to several factors. Density-based metrics are based directly on HU values and are thus susceptible to image acquisition noise and scanner HU calibration [5,20]. The Jacobian metric is calculated on the deformation field which in the case of ANTs is smoothed by B-Spline regularization [48]. Thus, Jacobian images appear smoother than their intensity-based analogs when no filtering is applied and are less prone to mis-

registration errors. This could explain why CT^{Jac} outperformed the other density based metrics for the voxel-wise analysis when no filtering was applied. However, recent work has shown the Jacobian metric to be numerically unstable in that small changes in the deformation field can give rise to larger changes in the ventilation distribution [8].

In general, CT^{SGV} was outperformed by CT^{HU} (section 3.5). Previously, Pennati et al. [37] compared CT^{SGV} with CT^{HU} in healthy normals and observed that CT^{SGV} provides more homogenous distributions of ventilation with minimal gravitational dependence. However, although this has been argued to be an advantage of CT^{SGV} in terms of decreasing variation in longitudinal evaluations and improving discrimination of healthy lung from diseased lung [37], it appears to mask some of the true underlying ventilation heterogeneity. Although gravitational effects have been traditionally considered a cause of ventilation heterogeneity in healthy subjects, recent studies have demonstrated heterogeneity within isogravitational planes [17]. Thus, CT^{HU} may provide a more accurate estimate of regional ventilation.

Despite notable similarities, none of the CT-ventilation images were perfectly matched to hyperpolarized gas MRI, with marked discrepancies in ventilation distributions observed. Quantitative analysis demonstrated consistently higher correlation of ^{3}He and ^{129}Xe MRI compared with the case when either gas was correlated to CT-ventilation. These results are analogous to a recent study comparing 4D-CT ventilation with paired ventilation/perfusion SPECT scans in a similar patient population to our study [19]. That study observed greater correlation of SPECT perfusion and ventilation than when any of the images were compared to 4D-CT ventilation.

There are multiple mechanisms that may be responsible for the differences between CT-based surrogates of ventilation and direct ventilation measurements from hyperpolarized gas MRI. Most notably, the assumption inherent in all the CT-ventilation metrics is that changes in lung density and volume between inflation levels are due solely to the influx of air, whilst lung perfusion remains regionally unaffected by lung inflation level [13]. However,

dual-energy CT has demonstrated that the regional distribution of pulmonary blood volume is sensitive to inflation level with differences between dependent and non-dependent regions [16]. As such, due to interference from perfusion, unlike hyperpolarized gas MRI, CT-ventilation surrogates do not provide direct measures of ventilation. Therefore, the correlation of CT-based surrogates of ventilation with hyperpolarized gas MRI may improve if additional images of regional blood volume at the same inflation levels as CT-ventilation are explicitly incorporated within the ventilation model. Currently, the efficacy of CT-ventilation for functional lung avoidance radiation therapy is being evaluated in three prospective clinical trials (NCT02528942, NCT02308709, NCT02843568). The outcomes of these studies could provide definitive evidence of the utility of this modality.

Discrepancies between techniques may also result from transient ventilation defects caused by, for example, a shift of mucus plugs during breath-hold [52], or due to delayed-filling ventilation defects related to the difference in breath-hold acquisition times; CT was acquired within 15 to 20 seconds whilst ^{3}He and ^{129}Xe-MRI were acquired within 7 and 15 seconds, respectively. Marshall et al. [33] have shown that some ventilation defects tend to resolve late during the course of a single 15 second breath-hold, due to collateral ventilation and the diffusive nature of ^{3}He gas.

4.2 Spatial correlation of ^{3}He and ^{129}Xe-MRI

To the best of our knowledge, this is also the first study to quantitatively assess the spatial correlation between ^{3}He and ^{129}Xe MRI at a voxel and regional level and thus may have parallel important implications to clinicians and scientists specialising in the field of hyperpolarized gas MRI. The hyperpolarized gases, ^{3}He and ^{129}Xe, exhibited stronger spatial correlation with each other than with CT-ventilation maps (with correlations also improving with increasing ROI size). Increased ventilation heterogeneity was observed for ^{129}Xe when compared with ^{3}He-MRI, which is consistent with recent studies comparing ^{129}Xe and ^{3}He-MRI in patients with asthma and COPD [30,44]. This may be explained by differences in diffusivity of the

gases; due to its lower molecular weight, ^{3}He has a much higher diffusion coefficient than ^{129}Xe and is thus more likely to penetrate partial obstructions within the acquisition time, leading to increased ventilation.

4.3 Study limitations

Differences currently exist in the acquisition procedures for the two gas MRI techniques, for example, the ability to obtain volumetric hyperpolarized gas and ^{1}H-MRI in a single breath-hold. However, progress towards overcoming technical limitations is underway in our research group, particularly the introduction of compressed sensing techniques [1] to accelerate the image acquisition and facilitate same-breath ^{129}Xe and ^{1}H-MRI.

5. Conclusion

Experimental validation of CT image registration based surrogates of ventilation is a necessary prerequisite to clinical implementation. To facilitate spatial correlation of CT-ventilation against hyperpolarized gas MRI, an image acquisition protocol and analysis strategy were developed and tested in a cohort of lung cancer patients undergoing radiotherapy. Moderately low correlations of CT at the voxel level were observed against hyperpolarized gas, increasing with larger regional analysis. Correlation between MRI and CT was significantly less than that of ^{3}He and ^{129}Xe-MRI, suggesting that CT-ventilation maps may not be measuring lung ventilation alone.

References

[1] **Anonymized**.

[2] Aliverti A, Pennati F, Salito C, et al. Regional lung function and heterogeneity of specific gas volume in healthy and emphysematous subjects. *Eur Respir J* 2013;41:1179-1188.

[3] Avants B, Tustison N, Song G, et al. A Unified Image Registration Framework for ITK. In: Dawant B, Christensen G, Fitzpatrick JM and Rueckert D, eds. Biomedical Image Registration, vol. 7359: Springer Berlin Heidelberg, 2012;pp. 266-275.

[4] Avants BB, Tustison NJ, Song G, et al. A reproducible evaluation of ANTs similarity metric performance in brain image registration. *Neuroimage* 2011;54:2033-2044.

[5] Boedeker KL, McNitt-Gray MF, Rogers SR, et al. Emphysema: effect of reconstruction algorithm on CT imaging measures. *Radiology* 2004;232:295-301.

[6] Brennan D, Schubert L, Diot Q, et al. Clinical validation of 4-dimensional computed tomography ventilation with pulmonary function test data. *Int J Radiat Oncol Biol Phys* 2015;92:423-429.

[7] Callahan J, Hofman MS, Siva S, et al. High-resolution imaging of pulmonary ventilation and perfusion with 68Ga-VQ respiratory gated (4-D) PET/CT. *Eur J Nucl Med Mol Imaging* 2014;41:343-349.

[8] Castillo E, Castillo R, Vinogradskiy Y, et al. The numerical stability of transformation-based CT ventilation. *Int J Comput Assist Radiol Surg* 2017;12:569-580.

[9] Castillo R, Castillo E, Martinez J, et al. Ventilation from four-dimensional computed tomography: density versus Jacobian methods. *Phys Med Biol* 2010;55:4661-4685.

[10] Castillo R, Castillo E, McCurdy M, et al. Spatial correspondence of 4D CT ventilation and SPECT pulmonary perfusion defects in patients with malignant airway stenosis. *Phys Med Biol* 2012;57:1855-1871.

[11] Christian JA, Partridge M, Nioutsikou E, et al. The incorporation of SPECT functional lung imaging into inverse radiotherapy planning for non-small cell lung cancer. *Radiother Oncol* 2005;77:271-277.

[12] Coxson HO, Mayo JR, Behzad H, et al. Measurement of lung expansion with computed tomography and comparison with quantitative histology. *J Appl Physiol (1985)* 1995;79:1525-1530.

[13] Ding K, Cao K, Fuld MK, et al. Comparison of image registration based measures of regional lung ventilation from dynamic spiral CT with Xe-CT. *Med Phys* 2012;39:5084-5098.

[14] Eslick EM, Bailey DL, Harris B, et al. Measurement of preoperative lobar lung function with computed tomography ventilation imaging: progress towards rapid stratification of lung cancer lobectomy patients with abnormal lung function. *Eur J Cardiothorac Surg* 2016;49:1075-1082.

[15] Fuld MK, Easley RB, Saba OI, et al. CT-measured regional specific volume change reflects regional ventilation in supine sheep. *J Appl Physiol* 2008;104:1177-1184.

[16] Fuld MK, Halaweish AF, Haynes SE, et al. Pulmonary perfused blood volume with dual-energy CT as surrogate for pulmonary perfusion assessed with dynamic multidetector CT. *Radiology* 2013;267:747-756.

[17] Glenny RW. Determinants of regional ventilation and blood flow in the lung. *Intensive Care Med* 2009;35:1833-1842.

[18] Guerrero T, Sanders K, Noyola-Martinez J, et al. Quantification of regional ventilation from treatment planning CT. *Int J Radiat Oncol Biol Phys* 2005;62:630-634.

[19] Hegi-Johnson F, Keall P, Barber J, et al. Evaluating the accuracy of 4D-CT ventilation imaging: First comparison with Technegas SPECT ventilation. *Med Phys* 2017;44:4045-4055.

[20] Hochhegger B, Irion KL, Marchiori E, et al. Reconstruction algorithms influence the follow-up variability in the longitudinal CT emphysema index measurements. *Korean J Radiol* 2011;12:169-175.
[21] Hogg JC Nepszy S. Regional lung volume and pleural pressure gradient estimated from lung density in dogs. *J Appl Physiol* 1969;27:198-203.
[22] **Anonymized**.
[23] **Anonymized**.
[24] **Anonymized**.
[25] **Anonymized**.
[26] **Anonymized**.
[27] Jacob RE, Lamm WJ, Einstein DR, et al. Comparison of CT-derived ventilation maps with deposition patterns of inhaled microspheres in rats. *Exp Lung Res* 2015;41:135-145.
[28] Kipritidis J, Hofman MS, Siva S, et al. Estimating lung ventilation directly from 4D CT Hounsfield unit values. *Med Phys* 2016;43:33.
[29] Kipritidis J, Siva S, Hofman MS, et al. Validating and improving CT ventilation imaging by correlating with ventilation 4D-PET/CT using 68Ga-labeled nanoparticles. *Med Phys* 2014;41:011910.
[30] Kirby M, Svenningsen S, Kanhere N, et al. Pulmonary ventilation visualized using hyperpolarized helium-3 and xenon-129 magnetic resonance imaging: differences in COPD and relationship to emphysema. *J Appl Physiol (1985)* 2013;114:707-715.
[31] Latifi K, Forster KM, Hoffe SE, et al. Dependence of ventilation image derived from 4D CT on deformable image registration and ventilation algorithms. *J Appl Clin Med Phys* 2013;14:4247.
[32] Levin DL, Schiebler ML Hopkins SR. Physiology for the pulmonary functional imager. *Eur J Radiol* 2017;86:308-312.
[33] **Anonymized**.
[34] Mathew L, Wheatley A, Castillo R, et al. Hyperpolarized (3)He magnetic resonance imaging: comparison with four-dimensional x-ray computed tomography imaging in lung cancer. *Acad Radiol* 2012;19:1546-1553.
[35] **Anonymized**.
[36] Patz S, Hersman FW, Muradian I, et al. Hyperpolarized (129)Xe MRI: a viable functional lung imaging modality? *Eur J Radiol* 2007;64:335-344.
[37] Pennati F, Salito C, Baroni G, et al. Comparison between multivolume CT-based surrogates of regional ventilation in healthy subjects. *Acad Radiol* 2014;21:1268-1275.
[38] Petersson J, Sanchez-Crespo A, Larsson SA, et al. Physiological imaging of the lung: single-photon-emission computed tomography (SPECT). *J Appl Physiol (1985)* 2007;102:468-476.
[39] Reinhardt JM, Ding K, Cao K, et al. Registration-based estimates of local lung tissue expansion compared to xenon CT measures of specific ventilation. *Med Image Anal* 2008;12:752-763.
[40] Seppenwoolde Y, Engelsman M, De Jaeger K, et al. Optimising radiation treatment plans for lung cancer using functional information. *Radiotherapy and Oncology* 2000;56.
[41] Siva S, Devereux T, Ball DL, et al. Ga-68 MAA Perfusion 4D-PET/CT Scanning Allows for Functional Lung Avoidance Using Conformal

Radiation Therapy Planning. *Technol Cancer Res Treat* 2016;15:114-121.
[42] Siva S, Thomas R, Callahan J, et al. High-resolution pulmonary ventilation and perfusion PET/CT allows for functionally adapted intensity modulated radiotherapy in lung cancer. *Radiother Oncol* 2015;115:157-162.
[43] **Anonymized**.
[44] Svenningsen S, Kirby M, Starr D, et al. Hyperpolarized (3) He and (129) Xe MRI: differences in asthma before bronchodilation. *J Magn Reson Imaging* 2013;38:1521-1530.
[45] **Anonymized**.
[46] **Anonymized**.
[47] **Anonymized**.
[48] Tustison NJ Avants BB. Explicit B-spline regularization in diffeomorphic image registration. *Front Neuroinform* 2013;7:39.
[49] Vinogradskiy Y, Koo PJ, Castillo R, et al. Comparison of 4-dimensional computed tomography ventilation with nuclear medicine ventilation-perfusion imaging: a clinical validation study. *Int J Radiat Oncol Biol Phys* 2014;89:199-205.
[50] **Anonymized**.
[51] **Anonymized**.
[52] **Anonymized**
[53] Yamamoto T, Kabus S, Klinder T, et al. Four-dimensional computed tomography pulmonary ventilation images vary with deformable image registration algorithms and metrics. *Med Phys* 2011;38:1348-1358.
[54] Yamamoto T, Kabus S, Lorenz C, et al. Pulmonary ventilation imaging based on 4-dimensional computed tomography: comparison with pulmonary function tests and SPECT ventilation images. *Int J Radiat Oncol Biol Phys* 2014;90:414-422.
[55] Zhang G, Huang TC, Dilling T, et al. Comments on 'Ventilation from four-dimensional computed tomography: density versus Jacobian methods'. *Phys Med Biol* 2011;56:3445-3446.
[56] Zhang GG, Huang TC, Dilling T, et al. Derivation of High-Resolution Pulmonary Ventilation Using Local Volume Change in Four-Dimensional CT Data. In: Dössel O and Schlegel W, eds. World Congress on Medical Physics and Biomedical Engineering, September 7 - 12, 2009, Munich, Germany, vol. 25/4: Springer Berlin Heidelberg, 2010;pp. 1834-1837.
[57] Zhang GG, Latifi K, Du K, et al. Evaluation of the DeltaV 4D CT ventilation calculation method using in vivo xenon CT ventilation data and comparison to other methods. *J Appl Clin Med Phys* 2016;17:5985.

Captions

Figure 1 Workflow of comparison method of CT-ventilation and gas MRI.

Figure 2 Corresponding coronal views of CT^{HU}, CT^{SGV} and CT^{Jac} (median filter radius: 3x3x3 voxels), and ^{3}He and ^{129}Xe-MRI after image registration for the best (top), intermediate (middle) and worst (bottom) cases of Spearman correlation of CT-ventilation with hyperpolarised gas MRI.

Figure 3 Box plot of Spearman correlation coefficients for CT-ventilation (CT^{HU}, median filter radius: 3x3x3 voxels) and hyperpolarized gas MRI at the voxel-level and for a range of ROIs.

Figure 4 Scatter plots of correlation coefficients of CT^{HU} against both ^{3}He (top) and ^{129}Xe (bottom) MRI with varying median filter radius.

Figure 5. Comparison of Spearman correlation coefficients for a range of CT-ventilation metrics with varying filter settings against ^{3}He (top) and ^{129}Xe-MRI (bottom).

Table 1 NSCLC patient characteristics

ACCEPTED MANUSCRIPT

ACCEPTED MANUSCRIPT

Table 1 NSCLC patient characteristics

Parameter	Value
Age (y)	63.64 ± 12.47 (34-77)
Sex	
Male	5 (45.45)
Female	6 (54.55)
COPD	5 (45.45)
Smoker	
Current	4 (36.36)
Former	7 (63.64)
FEV_1 (%-pred)	75.97 ± 24.48 (31.99-118.35)
FVC (%-pred)	103.10 ± 30.13 (59.05-155.74)
FEV_1/FVC (%-pred)	75.70 ± 21.70 (28.84-100.15)
DL_{CO} (%-pred)	53.19 ± 23.43 (8.47-89.80)
Clinical stage	
I	1 (9.09)
II	5 (45.45)
III	3 (27.27)
IV	2 (18.18)

Abbreviations: COPD = Chronic obstructive pulmonary disease; FEV_1 = forced expiratory volume in one second; FVC = forced vital capacity; DL_{CO} = diffusing capacity of the lung for carbon monoxide; %-pred = PFTs expressed as a percentage of a predicted value, based on the patient's age, height, and other demographic factors. Data are quoted as mean ± SD (range) with percentages in parenthesis. Former smokers are defined as those who have stopped smoking for at least three months prior to diagnosis.

ACCEPTED MANUSCRIPT

ACCEPTED MANUSCRIPT

Summary

This paper describes:

- an imaging protocol for acquiring pulmonary CT, ^{1}H, ^{3}He and ^{129}Xe-MRI with similar breath-holds and posture to facilitate accurate spatial comparison of CT-ventilation and hyperpolarized gas ventilation maps via deformable image registration
- a validation of CT-ventilation, generated from multi-inflation breath-hold CT, against hyperpolarized gas MRI
- a comparison of CT-ventilation against two commonly-used hyperpolarized noble gases (^{3}He and ^{129}Xe) for ventilation imaging
- a voxel-wise and ROI-based comparison of CT-ventilation and hyperpolarized gas MRI.

ACCEPTED MANUSCRIPT